JOURNAL OF GUIDANCE, CONTROL, AND DYNAMICS
Vol. 26, No. 6, November–December 2003

Observability of a Geosynchronous Spacecraft Attitude Determination System

Xipu Li* and Neil Goodzeit†
Lockheed Martin Commercial Space Systems, Newtown, Pennsylvania 18940

The observability is examined of a standard geosynchronous spacecraft attitude determination system that uses Earth and sun sensor measurements. The results show that the attitude determination error state, including the attitude and gyro bias errors, is entirely observable over the portion of the orbit where both sun and Earth sensor measurements are available. However, when the sun is outside the sun sensor window, the system is unobservable with a one-dimensional unobservable subspace. It is shown that the eigenvalue associated with this unobservable subspace is zero and that the corresponding eigenvector is an equilibrium line of the attitude determination system. The state vector converges to this equilibrium line from any initial state. This result has practical importance in spacecraft attitude control and may be used to speed the recovery from attitude determination anomalies. Numerical simulations and actual spacecraft flight data are included to illustrate the theory.

Nomenclature

$\boldsymbol{N}$	=	span$\{\boldsymbol{v}_1, \ldots, \boldsymbol{v}_n\}$, span $\boldsymbol{V}$
span $\boldsymbol{V}$	=	linear subspace spanned by vectors $\{\boldsymbol{v}_1, \ldots, \boldsymbol{v}_n\}$, where $\boldsymbol{V} = [\boldsymbol{v}_1 \ldots \boldsymbol{v}_n]$
$\|\boldsymbol{v}\|$	=	2 norm of vector $\boldsymbol{v}$

I. Introduction

FOR most geosynchronous spacecraft, the nominal Earth-pointing attitude is shown in Fig. 1. The spacecraft body yaw axis x is aligned with the anti-Earth (zenith) vector, the body roll axis y is aligned with the spacecraft velocity vector, and the body pitch axis z is aligned with the orbit normal vector. Earth sensors and sun sensors are commonly used for attitude determination (AD). The Earth sensor, which provides roll and pitch angle measurements, is normally mounted on the Earth-facing panel with its boresight aligned with the spacecraft's $-x$ axis. The sun sensor, which provides sun elevation and azimuth angles, is normally mounted such that its boresight points to the east or west direction. Figure 2 gives an example where the sun sensor is mounted with its boresight 55 deg from the $-x$ axis toward the east. The sun azimuth angle is defined as the angle between the $-x$ axis and the sun vector projection in the spacecraft x–y plane. The elevation angle is the angle between the sun vector and its projection on the x–y plane. The AD system needs two and only two well-separated reference vectors, such as the Earth and sun vectors, to determine a spacecraft's three-axis attitude.[1] Roughly speaking, the AD system uses Earth sensor data to update the spacecraft roll and pitch attitude and sun sensor elevation data to update the spacecraft yaw attitude. The sun sensor azimuth angle is not used because it provides the same information as the Earth sensor pitch angle. During normal operations, the Earth sensor is in constant view of the Earth; therefore, the roll and pitch attitude is updated continuously. However, the yaw attitude can only be updated for several hours each day when the sun is within a specified region of the sun sensor field of view referred to as the sun update window, for example, between azimuth angles of ± 35 deg measured from the sun sensor boresight. When the sun is outside of the update window, the yaw attitude is propagated using the gyro measured spacecraft angular rates.

This paper provides an analysis of the observability of the Earth and sun sensor referenced AD system. Although the analysis is based on the AD system of the A2100 spacecraft (Fig. 3), the theoretical results apply to general geosynchronous spacecraft AD systems. The analysis addresses two situations, one where the spacecraft uses both Earth sensor and sun sensor data for AD and another where it uses only Earth sensor data. The results show that the AD system is completely observable when both earth sensor and sun sensor data are available. However, when sun sensor data are not available, the system is not completely observable. The unobservable subspace is one dimensional and formed by a linear combination of the yaw attitude determination error and roll gyro bias estimation error with a ratio equal to the spacecraft orbit rate. This is consistent with the well-known yaw gyro compassing result presented in Ref. 2, which provides a comprehensive analysis of this subject. In contrast to Ref. 2, this paper determines the null vector of the observability matrix of the AD system, assuming a random walk gyro bias model, instead of a constant bias and exponentially correlated drift model. The random walk bias, although not an exact model of gyro behavior, is widely used for practical AD filter design applications. Furthermore, the analysis examines the stability of the unobservable subspace and shows that the eigenvalue associated with this unobservable subspace is zero and the corresponding eigenvector is an equilibrium line of the AD system. Additionally, applications of the theory to practical spacecraft operations problems are presented. The theory has been successfully applied to many A2100 in-orbit spacecraft to improve pointing performance in anomalous situations where the AD solution has been inadvertently corrupted.

The paper is organized as follows. The mathematical modeling and derivations are presented in Sec. II. In Sec. III, the AD observability analysis is given, and in Sec. IV, practical applications are demonstrated. Supporting numerical simulations and actual spacecraft flight data are provided in Sec. V.

II. Mathematical Model

The state-space representation for the AD system can be expressed as

$$\dot{\boldsymbol{x}}(t) = \boldsymbol{A}\boldsymbol{x}(t) + \boldsymbol{n}_s \tag{1}$$

$$\boldsymbol{y}(t) = \boldsymbol{C}\boldsymbol{x}(t) + \boldsymbol{n}_m \tag{2}$$

where $\boldsymbol{n}_s$ and $\boldsymbol{n}_m$ are system and measurement noise inputs, respectively.

A. Derivation of the State Equation

The state variable in Eq. (1) is a six-dimensional vector consisting of the three-axis AD error vector $\boldsymbol{e}$ and the three-axis gyro bias

Received 15 July 2002; presented at the AIAA Guidance, Navigation, and Control Conference, Monterey, CA, August 2002; revision received 20 May 2003; accepted for publication 7 June 2003.

*Senior Staff Engineer, Spacecraft Design Department. Member AIAA.
†Senior Principal Engineer, Chief Technology Office.

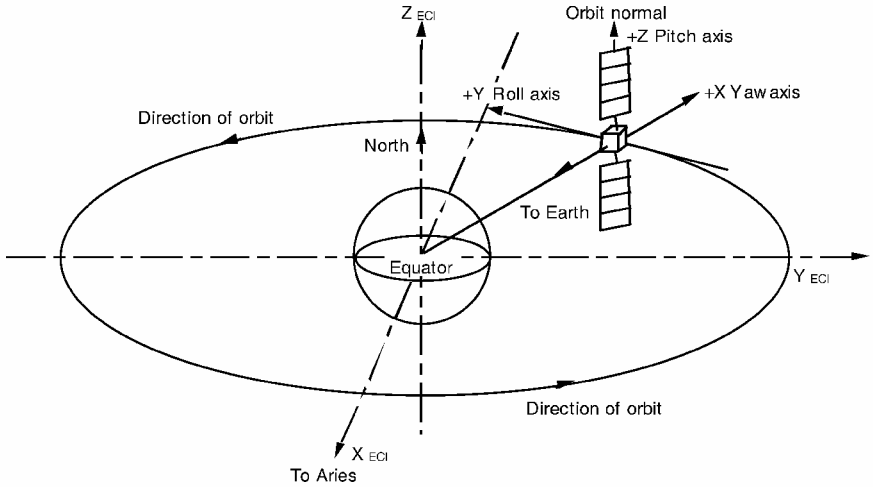

Fig. 1 Spacecraft coordinates and its nominal attitude.

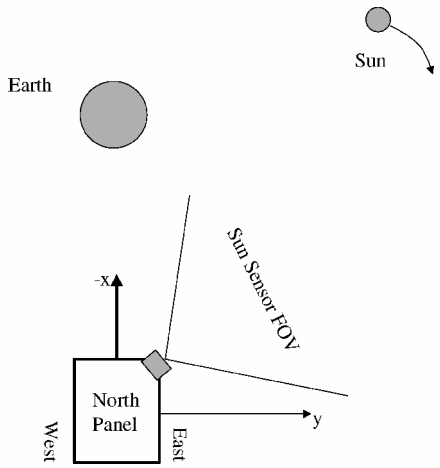

Fig. 2 Sun sensor field of view (FOV).

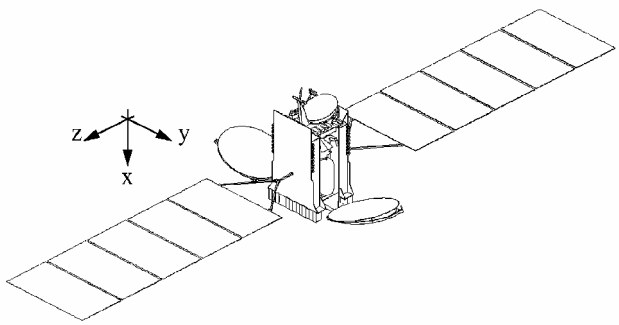

Fig. 3 A2100 spacecraft: X = yaw, Y = roll, and Z = pitch.

estimation error vector ω_{bias}:

$$\boldsymbol{x}(t) = \begin{bmatrix} \boldsymbol{e} \\ \omega_{\text{bias}} \end{bmatrix} = [\theta_x \quad \theta_y \quad \theta_z \quad \delta_x \quad \delta_y \quad \delta_z]^T \tag{3}$$

The AD error $\boldsymbol{e}$ is defined as the small angle rotation vector from the estimated spacecraft body coordinate frame to the true spacecraft body frame. The derivative of $\boldsymbol{e}$ can be expressed as[1,3]

$$\dot{\boldsymbol{e}} = -\boldsymbol{\omega} \times \boldsymbol{e} - \omega_{\text{bias}} + \boldsymbol{n}_1 = \boldsymbol{W}\boldsymbol{e} - \omega_{\text{bias}} + \boldsymbol{n}_1 \tag{4}$$

where $\boldsymbol{\omega} = [\omega_x \quad \omega_y \quad \omega_z]^T$ is the spacecraft body angular rate vector, $\boldsymbol{W}$ is the skew-symmetric angular rate matrix given by

$$\boldsymbol{W} = -\begin{bmatrix} 0 & -\omega_z & \omega_y \\ \omega_z & 0 & -\omega_x \\ -\omega_y & \omega_x & 0 \end{bmatrix} \tag{5}$$

and $\boldsymbol{n}_1$ is white noise. The gyro bias ω_{bias} is modeled as the random walk process[4] described by

$$\dot{\omega}_{\text{bias}} = \boldsymbol{n}_2 \tag{6}$$

where $\boldsymbol{n}_2$ is white noise that is independent of $\boldsymbol{n}_1$. When Eqs. (4) and (6) are combined, Eq. (1) can be written as

$$\begin{bmatrix} \dot{\boldsymbol{e}} \\ \dot{\omega}_{\text{bias}} \end{bmatrix} = \begin{bmatrix} \boldsymbol{W} & -\boldsymbol{I}_3 \\ \boldsymbol{0} & \boldsymbol{0} \end{bmatrix} \begin{bmatrix} \boldsymbol{e} \\ \omega_{\text{bias}} \end{bmatrix} + \begin{bmatrix} \boldsymbol{n}_1 \\ \boldsymbol{n}_2 \end{bmatrix} \tag{7}$$

where $\boldsymbol{I}_3$ is a 3×3 identity matrix.

B. Derivation of the Output Equation

The output vector $\boldsymbol{y}(t)$ in Eq. (2) consists of three measurement residuals:

$$\boldsymbol{y}(t) = \begin{bmatrix} y_1(t) \\ y_2(t) \\ y_3(t) \end{bmatrix} = \begin{bmatrix} \text{sun elevation residual} \\ \text{Earth roll residual} \\ \text{Earth pitch residual} \end{bmatrix} = z_m - z_{\text{est}} \tag{8}$$

where z_m is the attitude sensor measurement vector (sun elevation, Earth roll, and pitch angles) and z_{est} is the expected measurement vector calculated by the AD system. Because z_{est} is derived from the sun and Earth vectors transformed from the inertial reference frame to the body frame by using the onboard AD knowledge, it is also a function of the AD error $\boldsymbol{e}$. Equation (8) can be linearized and expressed in the form of Eq. (2):

$$\boldsymbol{y}(t) = z_m - z_{\text{est}}(\boldsymbol{e}) = z_m - \left[z_{\text{est}}(\boldsymbol{0}) - \frac{\partial z_{\text{est}}}{\partial \boldsymbol{e}}\boldsymbol{e} \right] = \frac{\partial z_{\text{est}}}{\partial \boldsymbol{e}}\boldsymbol{e}$$

$$= [\boldsymbol{C}_1 \quad \boldsymbol{0}]\boldsymbol{x} = \boldsymbol{C}\boldsymbol{x} \tag{9}$$

where $\boldsymbol{C}_1 = \partial z_{\text{est}}/\partial \boldsymbol{e}$ is a 3×3 Jacobian matrix consisting of the partial derivatives of the sensor measurements with respective to the AD errors.[4] Note that, in this equation, the sensor measurement error is not considered; therefore, $z_m = z_{\text{est}}(0)$. If we assume that the Earth sensor and sun sensor are mounted as described in Sec. I, then the C matrix in Eq. (9) can be written as

$$\boldsymbol{C} = \left[\begin{array}{ccc:ccc} -\sin\varphi(t) & -\cos\varphi(t) & 0 & 0 & 0 & 0 \\ 0 & 1 & 0 & 0 & 0 & 0 \\ 0 & 0 & 1 & 0 & 0 & 0 \end{array}\right] = [\boldsymbol{C}_1 \quad \boldsymbol{0}] \tag{10}$$

where $\varphi(t)$ is the sun azimuth angle. Note that Eq. (10) is a generic expression that applies when both the sun and the Earth are used for AD. When the sun is outside the sun update window (Fig. 2), the C matrix in Eq. (10) has only two rows (second and third rows).

C. Solution to the State Equation

The homogeneous solution to Eq. (1) is given by

$$\boldsymbol{x}(t) = \boldsymbol{\Phi}(t)\boldsymbol{x}(t_0) \tag{11}$$

where the state transition matrix $\boldsymbol{\Phi}(t)$ can be expressed in closed form using the Cayley–Hamilton theorem (see Refs. 1 and 5) as follows:

$$\boldsymbol{\Phi}(t) = \begin{bmatrix} \boldsymbol{\Phi}_1(t) & \boldsymbol{\Phi}_2(t) \\ \boldsymbol{0}_3 & \boldsymbol{I}_3 \end{bmatrix} \tag{12a}$$

$$\boldsymbol{\Phi}_1(t) = \boldsymbol{e}^{\boldsymbol{W}(t-t_0)} = \boldsymbol{I}_3 + a_1\boldsymbol{W} + a_2\boldsymbol{W}^2 \tag{12b}$$

$$\boldsymbol{\Phi}_2(t) = -\int_{t_0}^{t} \boldsymbol{e}^{\boldsymbol{W}(\tau-t_0)}\,\mathrm{d}\tau = b_0\boldsymbol{I}_3 + b_1\boldsymbol{W} + b_2\boldsymbol{W}^2 \tag{12c}$$

$$a_1 = \frac{\sin[\|\boldsymbol{\omega}\|(t-t_0)]}{\|\boldsymbol{\omega}\|} \tag{12d}$$

$$a_2 = \frac{1-\cos[\|\boldsymbol{\omega}\|(t-t_0)]}{\|\boldsymbol{\omega}\|^2} \tag{12e}$$

$$b_0 = -(t-t_0) \tag{12f}$$

$$b_1 = -a_2 \tag{12g}$$

$$b_2 = -\frac{\|\boldsymbol{\omega}\|(t-t_0) - \sin[\|\boldsymbol{\omega}\|(t-t_0)]}{\|\boldsymbol{\omega}\|^3} \tag{12h}$$

III. Observability Analysis

A. Observability with Both Sun and Earth Sensor Measurements

The following definition of linear system observability is standard and can be found in many textbooks, for example, Ref. 5.

Definition 1: A linear time-varying system $(\boldsymbol{A}, \boldsymbol{C})$ is completely observable on $[t_0, +\infty)$ if and only if

$$\boldsymbol{y}(t) = \boldsymbol{C}(t)\boldsymbol{x}(t) = \boldsymbol{C}(t)\boldsymbol{\Phi}(t)\boldsymbol{x}(t_0) \equiv \boldsymbol{0}, \qquad \text{for all } t \geq t_0 \tag{13}$$

implies

$$\boldsymbol{x}_0 = \boldsymbol{x}(t_0) = \boldsymbol{0} \tag{14}$$

Theorem 1: When both Earth and sun sensor measurements are available, the system $(\boldsymbol{A}, \boldsymbol{C})$ is completely observable.

Proof: When Eq. (12a) is used, Eq. (13) can be written as

$$\boldsymbol{y}(t) = [\boldsymbol{C}_1 \quad \boldsymbol{0}] \begin{bmatrix} \boldsymbol{\Phi}_1(t) & \boldsymbol{\Phi}_2(t) \\ \boldsymbol{0}_3 & \boldsymbol{I}_3 \end{bmatrix} \begin{bmatrix} \boldsymbol{x}_{01} \\ \boldsymbol{x}_{02} \end{bmatrix}$$

$$= \boldsymbol{C}_1[\boldsymbol{\Phi}_1(t)\boldsymbol{x}_{01} + \boldsymbol{\Phi}_2(t)\boldsymbol{x}_{02}] \equiv \boldsymbol{0}, \qquad \text{for all } t \geq t_0 \tag{15}$$

Because $\boldsymbol{C}_1$ is full rank when the sun is in the sun sensor update window, Eq. (15) is equivalent to

$$[\boldsymbol{\Phi}_1(t)\boldsymbol{x}_{01} + \boldsymbol{\Phi}_2(t)\boldsymbol{x}_{02}] \equiv \boldsymbol{0}, \qquad \text{for all } t \geq t_0 \tag{16}$$

When it is known that $\boldsymbol{\Phi}_1(t)$ is an orthogonal matrix, it is straightforward to prove that (Appendix A)

$$\boldsymbol{\Phi}_1^{-1}(t)\boldsymbol{\Phi}_2(t) = \boldsymbol{\Phi}_1^T(t)\boldsymbol{\Phi}_2(t) = \boldsymbol{\Phi}_2^T(t) = b_0\boldsymbol{I}_3 - b_1\boldsymbol{W} + b_2\boldsymbol{W}^2 \tag{17}$$

With Eq. (17), it can be proven (Appendix B) that the only solution that satisfies Eq. (16) for all time is $\boldsymbol{x}_{01} = \boldsymbol{x}_{02} = \boldsymbol{0}$. Therefore, the system of Eqs. (1) and (2) is completely observable when the sun is in the sun update window.

B. Observability with Only Earth Sensor Measurements

Without the sun sensor measurement, the system becomes time invariant, and the system observability can be examined directly from the following observability matrix:

$$\boldsymbol{O} = \begin{bmatrix} \boldsymbol{C} \\ \boldsymbol{CA} \\ \boldsymbol{CA}^2 \\ \cdots \\ \boldsymbol{CA}^5 \end{bmatrix} = \begin{bmatrix} \boldsymbol{C}_1 & \boldsymbol{0} \\ \boldsymbol{C}_1\boldsymbol{W} & -\boldsymbol{C}_1 \\ \boldsymbol{C}_1\boldsymbol{W}^2 & -\boldsymbol{C}_1\boldsymbol{W} \\ \cdots & \cdots \\ \boldsymbol{C}_1\boldsymbol{W}^5 & -\boldsymbol{C}_1\boldsymbol{W}^4 \end{bmatrix} \tag{18}$$

where

$$\boldsymbol{C} = \begin{bmatrix} 0 & 1 & 0 & 0 & 0 & 0 \\ 0 & 0 & 1 & 0 & 0 & 0 \end{bmatrix} = [\boldsymbol{C}_1 \quad \boldsymbol{0}] \tag{19}$$

Theorem 2: The system's unobservable subspace is one dimensional and is spanned by the null vector of $\boldsymbol{O}$:

$$\boldsymbol{v}_{\text{un}} = [1 \quad 0 \quad 0 \quad 0 \quad -\omega_z \quad \omega_y]^T \tag{20}$$

Proof: The rank 4 null space of $\boldsymbol{C}$ is

$$N_1 = \text{span} \begin{bmatrix} 1 & 0 & 0 & 0 \\ 0 & 0 & 0 & 0 \\ 0 & 0 & 0 & 0 \\ 0 & 1 & 0 & 0 \\ 0 & 0 & 1 & 0 \\ 0 & 0 & 0 & 1 \end{bmatrix} \tag{21}$$

It can also be seen that subspace

$$\boldsymbol{N}_2 = \text{span} \begin{bmatrix} \boldsymbol{I}_3 \\ \boldsymbol{W} \end{bmatrix} \tag{22}$$

is contained in the null space of

$$\begin{bmatrix} \boldsymbol{C}_1\boldsymbol{W} & -\boldsymbol{C}_1 \\ \boldsymbol{C}_1\boldsymbol{W}^2 & -\boldsymbol{C}_1\boldsymbol{W} \\ \cdots & \cdots \\ \boldsymbol{C}_1\boldsymbol{W}^5 & -\boldsymbol{C}_1\boldsymbol{W}^4 \end{bmatrix}$$

because

$$\begin{bmatrix} \boldsymbol{C}_1\boldsymbol{W} & -\boldsymbol{C}_1 \\ \boldsymbol{C}_1\boldsymbol{W}^2 & -\boldsymbol{C}_1\boldsymbol{W} \\ \cdots & \cdots \\ \boldsymbol{C}_1\boldsymbol{W}^5 & -\boldsymbol{C}_1\boldsymbol{W}^4 \end{bmatrix} \begin{bmatrix} \boldsymbol{I}_3 \\ \boldsymbol{W} \end{bmatrix} = \boldsymbol{0}$$

By inspection, we have

$$\boldsymbol{N} = \boldsymbol{N}_1 \cap \boldsymbol{N}_2 = \text{span}[1 \quad 0 \quad 0 \quad 0 \quad -\boldsymbol{\omega}_z \quad \boldsymbol{\omega}_y]^T \tag{23}$$

Note that $\boldsymbol{N}$ is contained in the null space of $\boldsymbol{O}$. On the other hand, it is straightforward to verify that

$$\begin{bmatrix} \boldsymbol{C}_1 & \boldsymbol{0} \\ \boldsymbol{C}_1\boldsymbol{W} & -\boldsymbol{C}_1 \\ \boldsymbol{C}_1\boldsymbol{W}^2 & -\boldsymbol{C}_1\boldsymbol{W} \end{bmatrix}$$

$$= \begin{bmatrix} 0 & 1 & 0 & 0 & 0 & 0 \\ 0 & 0 & 1 & 0 & 0 & 0 \\ -\omega_z & 0 & \omega_x & 0 & -1 & 0 \\ \omega_y & -\omega_x & 0 & 0 & 0 & -1 \\ \omega_x\omega_y & -\omega_x^2 - \omega_z^2 & \omega_y\omega_z & \omega_z & 0 & -\omega_x \\ \omega_x\omega_z & \omega_y\omega_z & -\omega_x^2 - \omega_y^2 & -\omega_y & \omega_x & 0 \end{bmatrix} \tag{24}$$

has a rank of 5, if either ω_z or ω_y is not zero. Therefore, $\boldsymbol{O}$ has at least a rank of 5, which means $\boldsymbol{N}$ is the unobservable subspace of the AD system.

During normal spacecraft operations, the spacecraft pitch rate is approximately equal to the orbit rate, that is, $\omega_z \approx \omega_0 = 15$ deg/h, and the spacecraft roll rate $\omega_y \approx 0$. Then Eq. (20) can be simplified, as

$$\boldsymbol{v}_{\text{un}} = [1 \quad 0 \quad 0 \quad 0 \quad -\omega_0 \quad 0]^T \tag{25}$$

The implication of Eq. (25) is that a linear combination of the yaw AD error and the roll gyro bias estimation error in the ratio of 1 to $-\omega_0$ is not observable in the Earth sensor measurements. Figure 4 and Eq. (26) further illustrate the following: If $\boldsymbol{x}(0) = \alpha \boldsymbol{v}_{\text{un}}$, where α is any real number, then

$$\boldsymbol{y}(t) = \boldsymbol{C}(t)\boldsymbol{\Phi}(t)\boldsymbol{x}(0) \equiv 0 \tag{26}$$

for all $t \geq 0$.

Theorem 3: Note that $\boldsymbol{v}_{\text{un}}$ is an eigenvector of $\boldsymbol{A}$, corresponding to an eigenvalue of zero.

The proof of this result is trivial by verifying the following equation:

$$\boldsymbol{A}\boldsymbol{v}_{\text{un}} = \boldsymbol{0} \tag{27}$$

Because this zero eigenvalue is unobservable, it is not possible to construct an estimator that will alter the dynamics of this "mode" of the AD system. This means that the zero eigenvalue and its eigenvector $\boldsymbol{v}_{\text{un}}$ will also be an eigenvalue and eigenvector pair of the closed-loop AD system. Hence, $\boldsymbol{v}_{\text{un}}$ defines an equilibrium line of the AD system. As shown in Fig. 5, starting from any initial condition, the AD state trajectory will converge to a point on this line where no further reduction in the yaw AD error x_1 and roll gyro bias estimation error x_5 is possible.

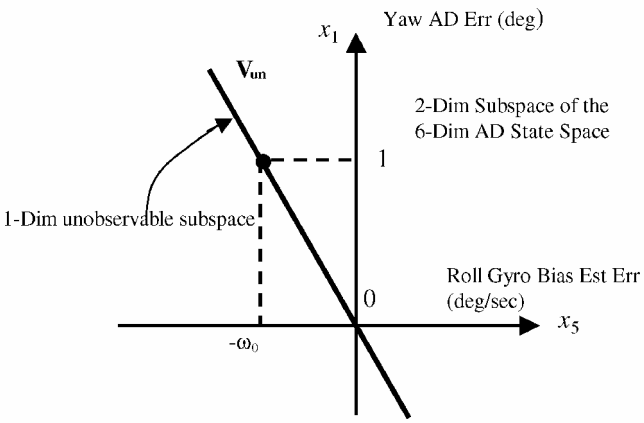

Fig. 4 State space of AD system.

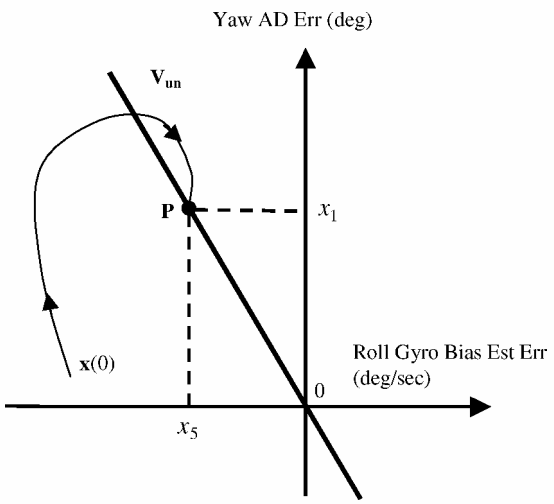

Fig. 5 State trajectory and equilibrium line.

IV. Applications

As discussed in the preceding section, when the sun is outside the sun update window, a linear combination of the yaw AD error and roll gyro bias estimation error is unobservable and cannot be removed. The yaw AD performance, or the position on line $\boldsymbol{v}_{\text{un}}$, is determined by two factors: 1) the gyro bias and 2) the initial AD state error at the beginning of the sun blind period. The gyro bias consists of a constant component and a time-varying component that may be modeled by a random walk noise process. The constant bias contributes a major portion to the gyro performance uncertainties. When it is assumed that the system has achieved steady state when the sun leaves the sun update window, then the AD error should be small, corresponding to a point on line $\boldsymbol{v}_{\text{un}}$ close to the origin. During the sun blind period, due to the effect of the time-varying gyro drift, the AD state trajectory will drift along the equilibrium line within a small neighborhood near the origin with high probability consistent with the required spacecraft AD performance. However, if an anomaly occurs within the sun blind region, the AD state may be corrupted in such a way that the AD state vector is disturbed from the equilibrium point and eventually converge to a different point on the line with a large AD error. As an example of this, Fig. 6 shows the impact on AD performance if the gyro bias estimate is corrupted outside of the sun update window. Before the event, the AD error has converged to point $\boldsymbol{P}_1$ with a small yaw residual AD error. The corruption of the gyro bias estimate moves the state vector from $\boldsymbol{P}_1$ to $\boldsymbol{P}_2$, and from there it eventually converges to $\boldsymbol{P}_3$ with a much larger yaw AD error.

Normally, full accuracy would not be recoverable until full state observability is achieved on entry to the sun update window. However, the results of the preceding section can be used to estimate and correct the yaw AD error during the sun blind period, without having to wait for entry to the sun update region. If we assume that no gyro failure is involved, which means that the earlier estimated gyro bias remains valid, then the roll gyro bias estimation error caused by the corruption is the difference between the current roll gyro bias estimate and the value before the event. Therefore, the yaw AD error can be estimated using Eq. (28), which is derived from the slope of $\boldsymbol{v}_{\text{un}}$:

$$\text{yaw AD error} = -\frac{\text{roll gyro bias estimation error}}{\text{nominal orbit rate}} \tag{28}$$

Note that Eq. (28) is the same as the equation derived using the gyro yaw compassing technique.[2] According to the developed theory, the yaw AD error can also be corrected as follows. With reference to Fig. 6, if the preevent gyro bias estimate is reset and the gyro bias updates are disabled, the state trajectory will jump to point $\boldsymbol{P}_4$

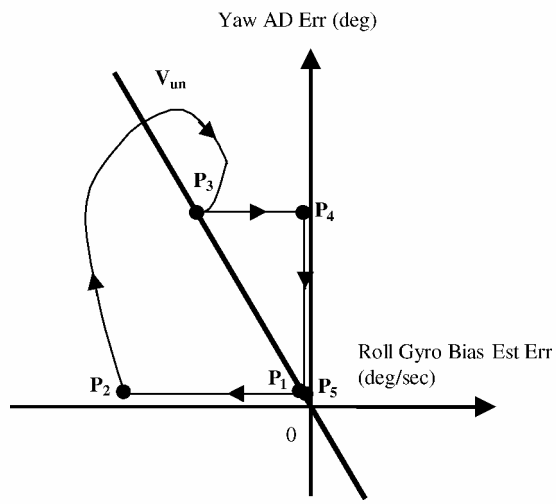

Fig. 6 Gyro bias corruption causes yaw AD error and recovery.

and remain along a vertical line corresponding to the error in the reset gyro bias. Note that the state trajectory will remain on this line, while the system converges, because the gyro bias estimates are held constant. Ultimately, the system will achieve steady state with a greatly reduced yaw AD error at $\boldsymbol{P}_5$, the intersection of the vertical line and the equilibrium line. As shown in the next section, this behavior is confirmed by both numerical simulation and actual spacecraft in-orbit data.

V. Simulations and Flight Data

In this section, numerical simulation results and flight data are presented to illustrate the theory developed in the preceding sections. Simulation case 1 illustrates the effect of a corruption of the gyro bias estimate outside the sun update window. As shown in Fig. 7, at 0.1 h from the start of the simulation, the gyro bias is reset to zero, which causes the AD system to reconverge with a 2.8-deg yaw AD error and a -4.55×10^{-5} deg/s gyro bias, that is, -1.9×10^{-4} deg/s roll gyro bias estimation error. The ratio of the yaw AD error to the roll gyro bias estimation error is close to negative orbit rate, which confirms that the trajectory converges to the equilibrium line shown in Fig. 5. At about 5.5 h, the sun leaves the sun sensor field of view, which sets the sun sensor elevation residual to zero, as shown in Fig. 7.

Simulation case 2 illustrates the yaw AD recovery process described in the preceding section. This case is same as case 1, except

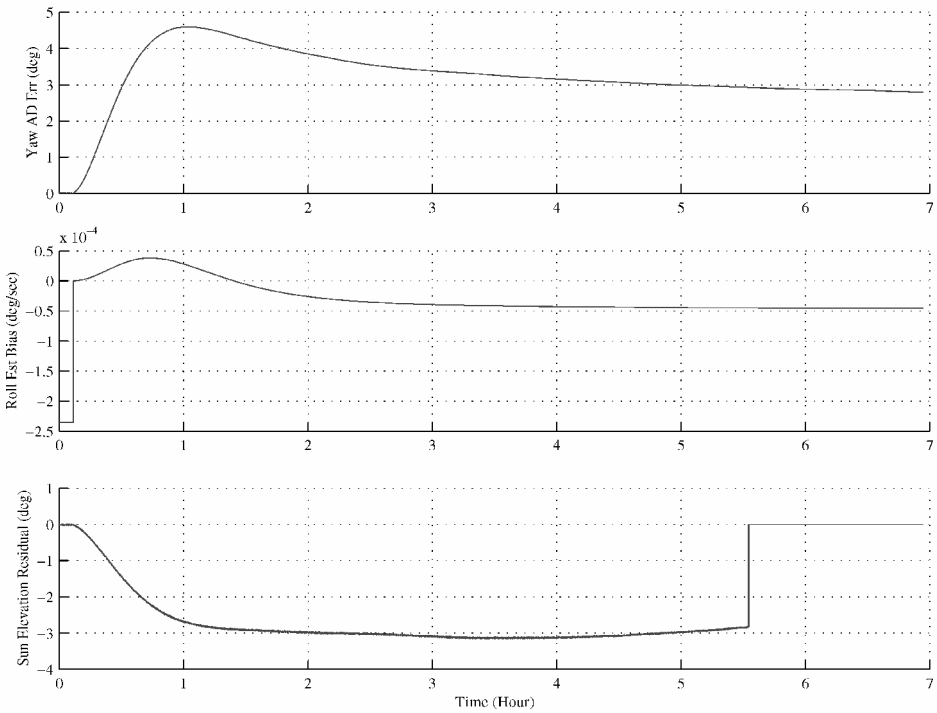

Fig. 7 Case 1: gyro bias reset at 0.1 h.

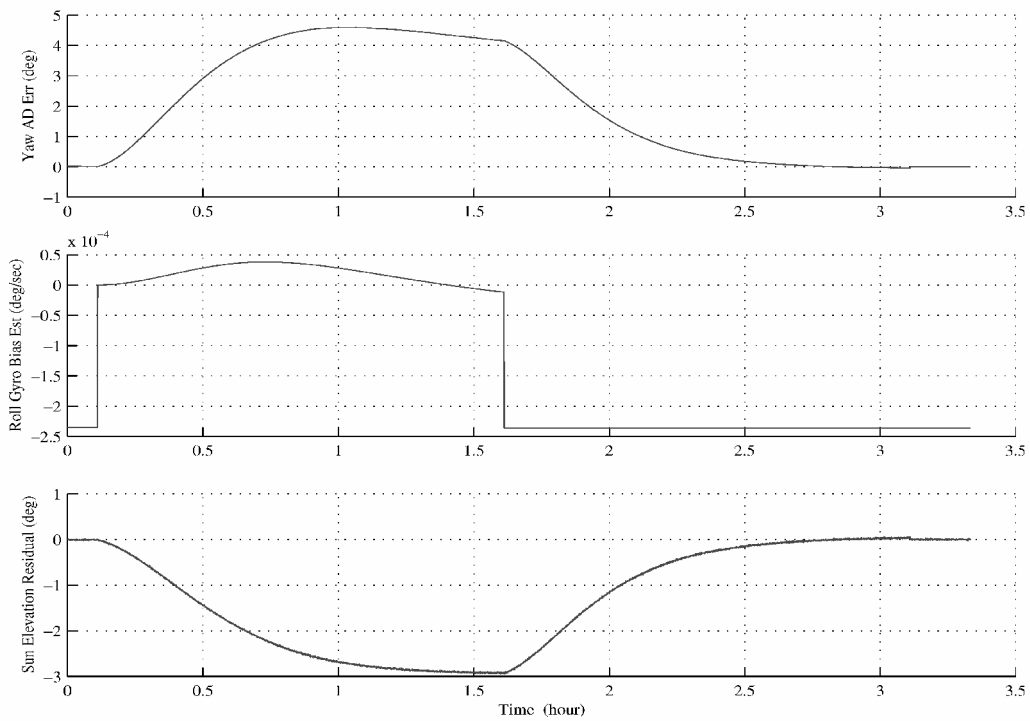

Fig. 8 Case 2: gyro bias and yaw attitude recovery.

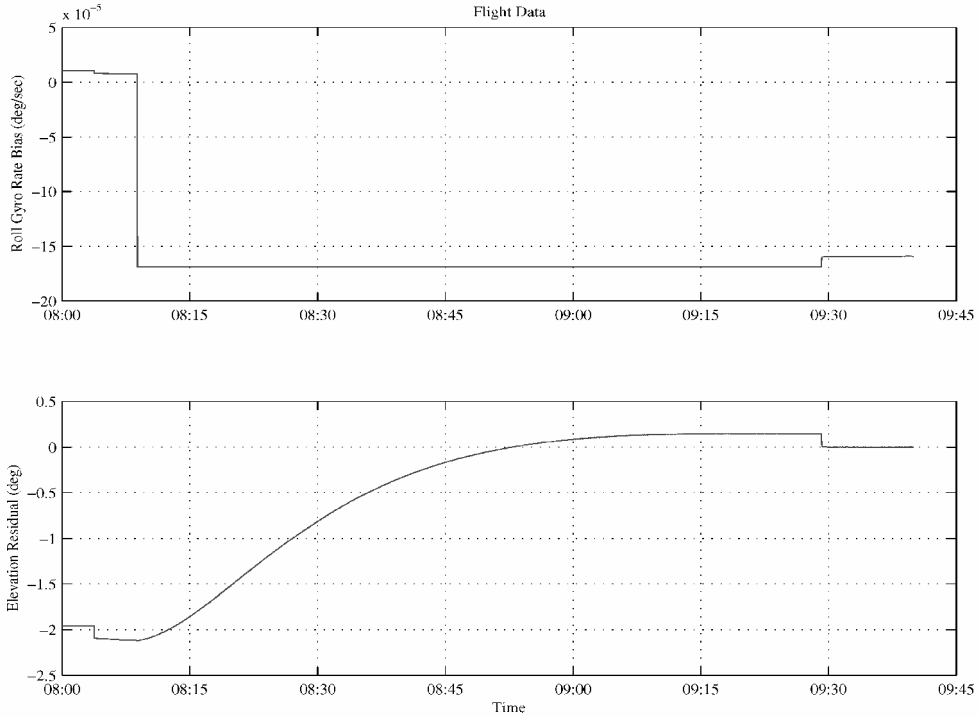

Fig. 9 Flight data from A2100 spacecraft.

that at 1.6 h into the simulation the gyro bias is reset to the nominal value and gyro bias updates are disabled. As shown in Fig. 8, this forces the state to converge with a greatly reduced yaw AD error (0.03 deg).

Figure 9 shows the yaw AD recovery process applied in-orbit during the preoperational test of an A2100 spacecraft. Figure 9 shows the sun sensor elevation residual and roll gyro bias response following inadvertent corruption of the gyro bias estimate. The response is shown starting at 0800 hrs after the bias corruption and with the AD system having reached steady state. The large yaw AD error can be seen from the large sun elevation residual (−2.1 deg). Note that, to replicate conditions in the sun blind region and yet retain yaw sensing, the test was performed in the sun update window with the sun update logic deliberately disabled. Therefore, although the true yaw AD error is unavailable, the sun sensor elevation residual provides an accurate indication of the yaw AD error; for example, see Figs. 7 and 8. After the preevent gyro bias is uploaded to the spacecraft at about 0809 hrs, the sun elevation residual starts decreasing as the yaw AD error is corrected. By 0920 hrs, the yaw AD error is reduced to less that 0.2 deg. At 0928 hrs, the sun sensor updates are reenabled, and the small residual yaw AD error is removed.

VI. Conclusions

Many geosynchronous communication satellites in service today include an onboard attitude determination system that processes Earth and sun sensor measurements to estimate the inertial attitude and gyro bias errors. When both Earth and sun sensor data are available, the attitude determination state is completely observable, and hence, recovery from AD state corruption events is rapid and automatic. However, over the portion of the orbit where sun sensor data is not available, the AD system must process Earth sensor data only. In this case, the system is unobservable with a one-dimensional unobservable subspace and zero eigenvalue. If disturbed, the system will, therefore, converge to a point on the line where the yaw AD error and roll gyro bias estimation error have a ratio equal to the orbit rate. When this result is used, it is possible to correct the resulting error by forcing the AD state to a point on the equilibrium line associated with the preevent gyro bias error. As illustrated by simulation and in-orbit test data, the approach has great practical value, allowing rapid recovery of AD accuracy, without having to wait for the availability of sun sensor data.

Appendix A: Properties of Transition Matrix 1

Because $\boldsymbol{W}^T = -\boldsymbol{W}$, Eq. (12b) indicates $\boldsymbol{\Phi}_1(t)$ is an orthogonal matrix, that is,

$$\boldsymbol{\Phi}_1^{-1}(t) = \boldsymbol{\Phi}_1^T(t) = \boldsymbol{I}_3 - a_1\boldsymbol{W} + a_2\boldsymbol{W}^2 \tag{A1}$$

Therefore,

$$\boldsymbol{\Phi}_1^{-1}(t)\boldsymbol{\Phi}_2(t) = \left(\boldsymbol{I}_3 - a_1\boldsymbol{W} + a_2\boldsymbol{W}^2\right)\left(b_0\boldsymbol{I}_3 + b_1\boldsymbol{W} + b_2\boldsymbol{W}^2\right) \tag{A2}$$

When

$$\boldsymbol{W}^3 = -\|\boldsymbol{\omega}\|^2\boldsymbol{W} \tag{A3a}$$

$$\boldsymbol{W}^4 = -\|\boldsymbol{\omega}\|^2\boldsymbol{W}^2 \tag{A3b}$$

and Eqs. (12d–12h) are used, it is straightforward to simplify Eq. (A2) to

$$\boldsymbol{\Phi}_1^{-1}(t)\boldsymbol{\Phi}_2(t) = b_0\boldsymbol{I}_3 - b_1\boldsymbol{W} + b_2 = \boldsymbol{\Phi}_2^T(t) \tag{A4}$$

Appendix B: Properties of Transition Matrix 2

A. Eigenvalues and Eigenvectors of $\boldsymbol{W}$

The skew symmetric matrix $\boldsymbol{W}$ has eigenvalues of $(0, j\|\boldsymbol{\omega}\|, -j\|\boldsymbol{\omega}\|)$ and satisfies

$$\boldsymbol{W}\boldsymbol{U} = \boldsymbol{U}\begin{bmatrix} 0 & 0 & 0 \\ 0 & 0 & \|\boldsymbol{\omega}\| \\ 0 & -\|\boldsymbol{\omega}\| & 0 \end{bmatrix} \tag{B1}$$

where

$$\boldsymbol{U} = [\boldsymbol{u}_1 \quad \boldsymbol{u}_2 \quad \boldsymbol{u}_3] \tag{B2a}$$

consists of three unit orthogonal vectors

$$\boldsymbol{u}_1 = \frac{1}{\|\boldsymbol{\omega}\|}\boldsymbol{\omega} \tag{B2b}$$

$$\boldsymbol{u}_2 = \frac{1}{\sqrt{2\left(\omega_x^2 + \omega_y^2\right)}\|\boldsymbol{\omega}\|}\begin{bmatrix} \omega_x\omega_z - \omega_y\|\boldsymbol{\omega}\| \\ \omega_y\omega_z + \omega_x\|\boldsymbol{\omega}\| \\ -\omega_x^2 - \omega_y^2 \end{bmatrix} \tag{B2c}$$

$$\boldsymbol{u}_3 = \frac{1}{\sqrt{2\left(\omega_x^2+\omega_y^2\right)}\|\boldsymbol{\omega}\|}\begin{bmatrix}\omega_x\omega_z+\omega_y\|\boldsymbol{\omega}\| \\ \omega_y\omega_z-\omega_x\|\boldsymbol{\omega}\| \\ -\omega_x^2-\omega_y^2\end{bmatrix} \tag{B2d}$$

Equation (B1) can be further expressed as

$$\boldsymbol{W}\boldsymbol{u}_1 = \boldsymbol{0} \tag{B3a}$$

$$\boldsymbol{W}\boldsymbol{u}_2 = -\|\boldsymbol{\omega}\|\boldsymbol{u}_3 \tag{B3b}$$

$$\boldsymbol{W}\boldsymbol{u}_3 = \|\boldsymbol{\omega}\|\boldsymbol{u}_2 \tag{B3c}$$

$$\boldsymbol{W}^2\boldsymbol{u}_2 = -\|\boldsymbol{\omega}\|^2\boldsymbol{u}_2 \tag{B3d}$$

$$\boldsymbol{W}^2\boldsymbol{u}_3 = -\|\boldsymbol{\omega}\|^2\boldsymbol{u}_3 \tag{B3e}$$

B. Solution to Equation (16)

Because $\{\boldsymbol{u}_1, \boldsymbol{u}_2, \boldsymbol{u}_3\}$ provides a set of basis vectors for the three-dimensional space, any initial condition $\boldsymbol{x}_{02}$ in Eq. (16) can be expressed as

$$\boldsymbol{x}_{02} = c_1\boldsymbol{u}_1 + c_2\boldsymbol{u}_2 + c_3\boldsymbol{u}_3 \tag{B4}$$

where $\{c_1, c_2, c_3\}$ are any real numbers. When Eqs. (12f–12h) and Eq. (17) are used, Eq. (16) can be written as

$$\boldsymbol{x}_{01} = -\boldsymbol{\Phi}_2^T\boldsymbol{x}_{02} = -\left(b_0\boldsymbol{I}_3 - b_1\boldsymbol{W} + b_2\boldsymbol{W}^2\right)(c_1\boldsymbol{u}_1 + c_2\boldsymbol{u}_2 + c_3\boldsymbol{u}_3) \tag{B5a}$$

$$= c_1(t-t_0)\boldsymbol{u}_1 \tag{B5b}$$

$$-(1/\|\boldsymbol{\omega}\|)(c_3\boldsymbol{u}_2 - c_2\boldsymbol{u}_3) \tag{B5c}$$

$$+(l/\|\boldsymbol{\omega}\|)\{\sin[\|\boldsymbol{\omega}\|(t-t_0)+\boldsymbol{\theta}]\}\boldsymbol{u}_2 \tag{B5d}$$

$$+(l/\|\boldsymbol{\omega}\|)\{\cos[\|\boldsymbol{\omega}\|(t-t_0)+\boldsymbol{\theta}]\}\boldsymbol{u}_3 \tag{B5e}$$

where $l = \sqrt{(c_2^2 + c_3^2)}$ and $\boldsymbol{\theta} = \arctan(c_3/c_2)$.

Equation (B-5) implies that $\boldsymbol{x}_{01}$ is in general a function of time. The first term [Eq. (B5b)] shows that $\boldsymbol{x}_{01}$ linearly increases in the negative $\boldsymbol{u}_1$ direction. The second, third, and fourth terms [Eqs. (B5c), (B5d), and (B5e)] show that the projection of $\boldsymbol{x}_{01}$ in the $\boldsymbol{u}_2 - \boldsymbol{u}_3$ plane moves along a circle that is centered at $1/\|\boldsymbol{\omega}\|(c_3\boldsymbol{u}_2 - c_2\boldsymbol{u}_3)$ and has a radius of $l/\|\boldsymbol{\omega}\|$. Therefore, for $\boldsymbol{x}_{01}$ to be a constant vector, $\{c_1, c_2, c_3\}$ have to be all zeros, which means $\boldsymbol{x}_{01} = \boldsymbol{x}_{02} = \boldsymbol{0}$.

Acknowledgments

The authors are grateful to M. Patel, M. Arbogast, K. Rogers, S. Ratan, C. Jayaraman, and J. Desimpel of Lockheed Martin Missiles and Space for their thoughtful insights and valuable discussions.

References

[1] Li, X., Boka, J. B., and Throckmorton, A. J., "Stability Analysis on Earth Observing System AM-1 Spacecraft Attitude Determination," *Journal of Guidance, Control, and Dynamics*, Vol. 20, No. 5, 1997, p. 1042.

[2] Bryson, A. E., and Kortum, W., "Estimation of the Local Attitude of Orbiting Spacecraft," *Automatica*, Vol. 7, 1971, pp. 163–180.

[3] Murrell, J. W., "Precision Attitude Determination for Multi-Mission Spacecraft," AIAA Paper 78-1248, Aug. 1978.

[4] Gelb, A. (ed.), *Applied Optimal Estimation*, MIT Press, Cambridge, MA, 1974, p. 79.

[5] Kwakernaak, H., and Sivan, R., *Linear Optimal Control Systems*, Wiley-Interscience, New York, 1972, p. 66.